

Propagation dynamics of relativistic electromagnetic solitary wave as well as modulational instability in plasmas

Rong-An Tang(唐荣安)†, Tiao-Fang Liu(刘调芳)\cclink, Xue-Ren Hong(洪学仁), Ji-Ming Gao(高吉明), Rui-Jin Cheng(程瑞锦), You-Lian Zheng(郑有莲), and Ju-Kui Xue(薛具奎)

Citation: Chin. Phys. B, 2021, 30 (**1**): 015201. DOI: 10.1088/1674-1056/abb224
Journal homepage: http://cpb.iphy.ac.cn; http://iopscience.iop.org/cpb

What follows is a list of articles you may be interested in

Research of influence of the additional electrode on Hall thruster plume by particle-in-cell simulation

Xi-Feng Cao(曹希峰), Hui Liu(刘辉), Da-Ren Yu(于达仁)
Chin. Phys. B, 2020, 29 (**9**): 095204. DOI: 10.1088/1674-1056/aba2e3

Spontaneous growth of the reconnection electric field during magnetic reconnection with a guide field: A theoretical model and particle-in-cell simulations

Kai Huang(黄楷), Quan-Ming Lu(陆全明), Rong-Sheng Wang(王荣生), Shui Wang(王水)
Chin. Phys. B, 2020, 29 (**7**): 075202. DOI: 10.1088/1674-1056/ab8da0

Formation of electron depletion layer and parallel electric field in the separatrix region of anti-parallel magnetic reconnection

Zisheng Li(李子圣), Huanyu Wang(王焕宇), Xinliang Gao(高新亮)
Chin. Phys. B, 2019, 28 (**7**): 075203. DOI: 10.1088/1674-1056/28/7/075203

Numerical simulation on modulational instability of ion-acoustic waves in plasma

Yi-Rong Ma(马艺荣), Lie-Juan Li(李烈娟), Wen-Shan Duan(段文山)
Chin. Phys. B, 2019, 28 (**2**): 025201. DOI: 10.1088/1674-1056/28/2/025201

Generation of high quality ion beams through the stable radiation pressure acceleration of the near critical density target

Xue-Ren Hong(洪学仁), Wei-Jun Zhou(周伟军), Bai-Song Xie(谢柏松), Yang Yang(杨阳), Li Wang(王莉), Jian-Min Tian(田建民), Rong-An Tang(唐荣安), Wen-Shan Duan(段文山)
Chin. Phys. B, 2017, 26 (**6**): 065203. DOI: 10.1088/1674-1056/26/6/065203

Propagation dynamics of relativistic electromagnetic solitary wave as well as modulational instability in plasmas*

Rong-An Tang(唐荣安)†, Tiao-Fang Liu(刘调芳)‡, Xue-Ren Hong(洪学仁), Ji-Ming Gao(高吉明), Rui-Jin Cheng(程瑞锦), You-Lian Zheng(郑有莲), and Ju-Kui Xue(薛具奎)

Key Laboratory of Atomic and Molecular Physics and Functional Materials of Gansu Province, College of Physics and Electronic Engineering, Northwest Normal University, Lanzhou 730070, China

(Received 1 June 2020; revised manuscript received 31 July 2020; accepted manuscript online 25 August 2020)

By one-dimensional particle-in-cell (PIC) simulations, the propagation and stability of relativistic electromagnetic (EM) solitary waves as well as modulational instability of plane EM waves are studied in uniform cold electron-ion plasmas. The investigation not only confirms the solitary wave motion characteristics and modulational instability theory, but more importantly, gives the following findings. For a simulation with the plasma density 10^{23} m^{-3} and the dimensionless vector potential amplitude 0.18, it is found that the EM solitary wave can stably propagate when the carrier wave frequency is smaller than 3.83 times of the plasma frequency. While for the carrier wave frequency larger than that, it can excite a very weak Langmuir oscillation, which is an order of magnitude smaller than the transverse electron momentum and may in turn modulate the EM solitary wave and cause the modulational instability, so that the solitary wave begins to deform after a long enough distance propagation. The stable propagation distance before an obvious observation of instability increases (decreases) with the increase of the carrier wave frequency (vector potential amplitude). The study on the plane EM wave shows that a modulational instability may occur and its wavenumber is approximately equal to the modulational wavenumber by Langmuir oscillation and is independent of the carrier wave frequency and the vector potential amplitude. This reveals the role of the Langmuir oscillation excitation in the inducement of modulational instability and also proves the modulational instability of EM solitary wave.

Keywords: electromagnetic solitary wave, particle-in-cell (PIC) simulation, modulational instability, Langmuir oscillation

PACS: 52.35.Sb, 52.35.–g, 52.35.Mw, 52.38.–r **DOI:** 10.1088/1674-1056/abb224

1. Introduction

The nonlinear interaction between an intense electromagnetic (EM) pulse and plasmas is of great interest in various fundamental research and technological applications, including harmonic generation,[1–3] self-focusing,[4–6] wakefield generation,[7,8] relativistic optical guiding,[9–11] x-ray,[12] laser pulse frequency shifting,[13] pulse compression,[14] relativistic EM soliton propagation.[15–19] Among spectacular phenomena in nonlinear interactions, relativistic EM solitary waves have attracted a great deal of attention in a fundamental point of view, also due to their possible applications in inertial confinement fusion and the charged particle acceleration.[20–23] In addition, as an important nonlinear process, modulational instability is closely related to propagation of EM waves. The development of modulational instability may induce a variety of nonlinear behaviors such as field collapse and localization, filamentation, envelope solitons, envelope shocks.[24–27]

As displayed in Refs. [28,29], nearly 25–40 percent of the laser pulse energy goes into the generation of well localized concentrations of electromagnetic energy in the form of solitary waves or soliton-like structures, which can play a significant role in the laser plasma interaction process. The EM solitary waves have been observed in experiment,[30,31] and the existence of relativistic solitary waves was predicted theoretically in plasmas[16,32–35] and found in the short and high intensity laser pulse interaction with under dense plasmas by particle-in-cell (PIC) simulations.[28,29,36–44] The EM solitary waves can be popularly regarded as the EM waves trapped locally in plasmas, and are generally interpreted as the result of the counterbalance between the nonlinearity and dispersion in nonlinear media. Similarly, modulational instability is also seen to be the outcome of the interplay between nonlinearity and dispersive effects. It is a symmetry-breaking instability so that the perturbation to the laser pulse experiences exponential growth, and this leads to beam breakup in either space or time. The modulational instability is general in plasmas[45–51] and other nonlinear media.[52,53]

In recent decades, relativistic EM solitary waves have been widely studied.[16,34,35,54–68] Theoretically, the existences and characteristics of different types of solitary wave in plasmas have attracted attention.[16,34,35,54–59] The one-

*Project supported by the National Natural Science Foundation of China (Grant Nos. 11765017, 11865014, 11847304, and 11764039), the Scientific Research Project of Gansu Higher Education, China (Grant No. 2019B-034), and the Science and Technology Project of Guizhou Province, China (Grant No. Qiankehe-LH-[2017]7008).

†Corresponding author. E-mail: tangra79@163.com

‡Corresponding author. E-mail: LTF25975@163.com

© 2021 Chinese Physical Society and IOP Publishing Ltd

dimension (1D) relativistic standing solitary waves in unmagnetized plasmas at arbitrary temperatures were investigated in Refs. [35,54,55] These results showed that the amplitude and shape of standing solitary waves depend on the plasma temperature. In Ref. [56], the dissipative EM stationary and breathing solitary waves in electron-ion collisional plasmas were studied by using the multi-scale reduced perturbation method. The parameter regions for the existence of the solitary waves were given and the dependence of the shape of the solitary waves on the parameters was discussed. Electromagnetic envelope solitary waves were also studied in warm plasmas,[34] magnetized pari plasmas,[57] magnetized electron-ion plasmas[58] and unmagnetized electron-positron plasmas.[59] It was shown that electromagnetic envelope solitary waves can exist in these plasmas under appropriation conditions, and their shapes and group velocities are related to plasma temperatures,[34] magnetic field strength[57,58] and the number density ratio of positrons to electrons.[59] With the development of computing technology, the simulation of a system of several partial differential equations can be performed, for example, the fluid simulation. The fluid simulation can be used to solve some problems that are difficult or cannot be dealt with in theory, such as the instability,[61,63] the generation[66–68] of solitary waves and the interaction[64,65] between them. For the instability of EM solitary waves, some works have been carried out theoretically by numerical simulation of wave equation before using fluid simulation. The stability of 1D relativistic standing solitary waves with single hump was primitively studied in plasmas theoretically.[60] Their results showed that the small-amplitude linearly polarized solitary waves within the weakly relativistic model are stable and are verified by the numerical simulation of the wave equation (i.e., generalized nonlinear Schrödinger equation). Based on the similar wave equation, the evolution of single hump envelope solitary wave was simulated by means of the split-step Fourier method with a fourth-order Runge–Kutta method to advance in time,[58] and it was found that the amplitude and shape of the solitary wave propagated in magnetized plasmas do not change substantially. A fluid simulation about multihump standing solitary waves[61] indicated that the multihump standing solitary waves are stable in electronic time scale, but become unstable as soon as the motion of ions is taken into account. A following theoretical investigation revealed that the instability of these multihump standing solitary waves can be understood on the basis of the simulated Raman scattering phenomenon and the occurrence of density bursts in the trailing edge of the modulated structures are a manifestation of an explosive instability arising from a nonlinear phase mixing mechanism.[62] By fluid simulation, the study of travelling single hump and multihump solitary waves in cold electron-ion plasmas showed that the single hump solitary waves are stable in the propagation process, while the multihump solitary waves are unstable and the instability occurs first from the trailing edge.[63]. It is noted that the single hump EM solitary waves seem to be always stable in the above investigations. More powerful than fluid simulation, the PIC technology was proposed and applied in the field of electromagnetic field and plasmas in recent decades.[28,29,69–71] PIC simulation is different from the simulation of macroscopic equations in the usual numerical methods, but uses macro particles to represent the real charged particles and simulate the self-consistent variation of particles positions and electromagnetic fields,[72] which is closer to the real physical process and helped researchers to achieve much progress that is difficult for other methods. Recently, PIC technology has begun to be used in the study of EM solitary waves in plasmas. It was found that the EM solitary waves can be formed by the interaction of two-color laser and plasma,[73] and can also be excited by the linearly polarized laser in overdense plasmas.[74] Up to date, we do not see a report about the EM solitary wave instability and the test of the EM solitary wave characteristic theory by PIC simulation.

In addition, some progress has been made in the study for modulational instability of plane EM waves in plasmas. For example, the effects of different physical parameters on the EM wave modulational instability in plasmas were studied in Refs. [27,58,75,76]. These results showed that the instability growth rate and the wavenumber range are related to plasma temperatures,[75] magnetic field strength[58,76] and the number density ratio of positrons to electrons.[27] In Ref. [77], the modulational instability of coupled plane EM waves in plasmas was studied and the dependence of the instability growth rate and the wavenumber range on the system parameters was discussed. Although many important results have been obtained, they are only in theory. We have not seen a report on the numerical test of the modulational instability of EM waves in plasmas.

Therefore, based on the above research status, we decide to test the theories of solitary wave characteristics and modulational instability, and study the solitary wave stability in plasmas by PIC simulation. As a beginning and for simplicity, we take the theories of a 1D relativistic EM solitary wave and modulational instability in uniform cold electron-ion plasmas as our test object, and perform more in-depth study of the solitary wave propagation dynamics (including stability) and modulational instability in this paper. Here we use the one-dimensional (1D) PIC technology to simulate a linear polarization electromagnetic wave propagating in one direction. The results cannot just confirm the correctness of the solitary wave motion characteristic and modulational instability theory but show the main physical parameters influencing the stable propagation of EM waves in uniform cold electron-ion plasmas. More importantly, the simulation gives the three find-

ings: (1) It is found for the first time that the stable propagation of envelope solitary waves may be destroyed by modulational instability. It was previously thought that a monochromatic plane wave may eventually develop into several solitary waves due to modulational instability. However, this work completely renews the understanding of the relationship between solitary wave and modulational instability. (2) The simulation reveals the importance of the excitation of the Langmuir oscillation to the modulational instability and the stable propagation of EM solitary waves, which has never been noticed in the corresponding theory before. (3) The simulation also refreshes our knowledge of the stability of single hump EM solitary waves, noting the previous common stable results without the consideration of electron modulation. The studies of the modulational instability in this paper have some specific applications. For example, it could be used for the design of plasma modulators for the generation of broadband high-power laser pulses,[78] which play a positive role in the suppression of laser-plasma instabilities in ICF. Further, the modulational instability can result in the self-compression effect of an intense laser pulse.[79] This could be used for the amplification of high-power laser pulses for broad applications.

The paper is arranged as follows: In Section 2, the basic model is listed, the main theoretical results of the EM envelope solitary wave and modulational instability are given by observable parameters suitable for PIC simulation. In Section 3, propagation dynamics and stability of EM solitary wave are carried out by PIC simulation. In Section 4, the PIC simulation results of modulational instability are given and discussed. Conclusions are briefly presented in Section 5.

2. Basic model as well as solitary wave solution and modulational instability

2.1. Theoretical model

The main purpose of the present article is to study the propagation dynamics of relativistic EM wave in uniform cold electron-ion plasmas. Assuming that the ion is immobile and that a linearly polarized electromagnetic pulse propagates along the $\hat{x}$ axis, applying the Coulomb specification $(\nabla\cdot\boldsymbol{A}=0)$,[80] the governing equations of the electromagnetic wave based on relativistic fluid model can be written in the form[56,80]

$$\frac{\partial^2\tilde{\boldsymbol{A}}}{\partial\tilde{x}^2}-\frac{\partial^2\tilde{\boldsymbol{A}}}{\partial\tilde{t}^2}=\frac{\partial^2\tilde{\phi}}{\partial\tilde{t}\partial\tilde{x}}\hat{x}+\frac{\tilde{n}}{\gamma}\tilde{\boldsymbol{P}}, \tag{1}$$

$$\frac{\partial^2\tilde{\phi}}{\partial\tilde{x}^2}=\tilde{n}-1, \tag{2}$$

$$\frac{\partial\tilde{n}}{\partial\tilde{t}}+\frac{\partial(\tilde{n}\tilde{u})}{\partial\tilde{x}}=0, \tag{3}$$

$$\frac{\partial(\tilde{\boldsymbol{P}}-\tilde{\boldsymbol{A}})}{\partial\tilde{t}}=\frac{\partial(\tilde{\phi}-\gamma)}{\partial\tilde{x}}\hat{x}+\tilde{\boldsymbol{V}}\times(\frac{\partial}{\partial\tilde{x}})\hat{x}\times(\tilde{\boldsymbol{P}}-\tilde{\boldsymbol{A}}), \tag{4}$$

$$\gamma=\sqrt{1+|\tilde{\boldsymbol{P}}|^2}, \tag{5}$$

where $\tilde{\boldsymbol{P}}=\tilde{p}_y(x,t)\hat{y}+\gamma\tilde{u}(x,t)\hat{x}$ is the electron momentum, $\tilde{p}_y$ is the transverse electron momentum, $\tilde{u}$ is the longitudinal component of the electron velocity, γ is the relativistic factor, $\tilde{\boldsymbol{V}}=\tilde{\boldsymbol{P}}/\gamma$ is the fluid velocity, $\tilde{\boldsymbol{A}}=\tilde{A}(x,t)\hat{y}$ and $\tilde{\phi}$ are the vector and scalar potentials of the electromagnetic wave, $\tilde{n}$ is the plasma density. Equations (1)–(5) have been normalized, and the normalization methods of the physical parameters are as follows:

$$\begin{aligned}&\tilde{\boldsymbol{A}}=\frac{e}{mc^2}\boldsymbol{A},\quad\tilde{\phi}=\frac{e}{mc^2}\phi,\quad\tilde{n}=\frac{n}{n_0},\\&\tilde{\omega}=\frac{\omega}{\omega_{\rm pe}},\quad\tilde{k}=\frac{k}{k_{\rm pe}},\quad\tilde{\boldsymbol{P}}=\frac{\boldsymbol{P}}{mc},\quad\tilde{\boldsymbol{v}}=\frac{\boldsymbol{v}}{c},\\&\tilde{t}=\omega_{\rm pe}t,\quad\tilde{x}=\frac{\omega_{\rm pe}}{c}x,\quad\tilde{\boldsymbol{E}}=\frac{e}{mc\omega_{\rm pe}}\boldsymbol{E},\end{aligned} \tag{6}$$

where $\omega_{\rm pe}=(n_0e^2/\varepsilon_0m)^{1/2}$ is the plasma frequency, n_0 is the initial plasma density, m is the electron mass, e is the charge of the electron, ε_0 is the dielectric constant in vacuum, $k_{\rm pe}=\omega_{\rm pe}/c$ is the plasma wave number, c is the velocity of light in vacuum, and $\boldsymbol{E}$ is the electric field.

Integrating Eq. (4) gives[56]

$$\tilde{p}_y=\tilde{A}. \tag{7}$$

In the weak relativistic approximation $(\tilde{A}\ll1)$[34,81,82] and by using the multiscale perturbation method, Eqs. (1)–(5) and (7) give the following total vector potential[56]

$$\tilde{A}(x,t)\simeq\varepsilon\tilde{\psi}(x,t)\,{\rm e}^{{\rm i}(\tilde{k}\tilde{x}-\tilde{\omega}\tilde{t})}+{\rm c.c.}, \tag{8}$$

where ε is a small dimensionless parameter, c.c. denotes complex conjugation, $\tilde{k}$ and $\tilde{\omega}$ are the frequency and wave number of the carrier wave, which are normalized by $\omega_{\rm pe}$ and $k_{\rm pe}=\omega_{\rm pe}/c$, respectively, and satisfy the linear dispersion relation approximately

$$\tilde{\omega}^2=\tilde{k}^2+1, \tag{9}$$

and the slowly varying amplitude $\tilde{\psi}(x,t)$ obeys the nonlinear Schrödinger equation

$${\rm i}\frac{\partial\tilde{\psi}}{\partial\tilde{\tau}}+D\frac{\partial^2\tilde{\psi}}{\partial\tilde{\eta}^2}+N|\tilde{\psi}|^2\tilde{\psi}=0, \tag{10}$$

where $\tilde{\eta}=\varepsilon(\tilde{x}-\tilde{v}_{\rm g}\tilde{t})$, $\tilde{\tau}=\varepsilon^2\tilde{t}$, $\tilde{v}_{\rm g}\approx\tilde{k}/\tilde{\omega}$ is the group velocity of electromagnetic wave, D and N represent the dispersion coefficient and the nonlinear coefficient respectively, and their expressions are as follows:

$$D=\frac{1}{2\tilde{\omega}^3}, \tag{11}$$

$$N=\frac{3}{4\tilde{\omega}}-\frac{\tilde{\omega}^2-1}{\tilde{\omega}^2(4\tilde{\omega}^2-1)}. \tag{12}$$

When the collision effect is not considered in Ref. [56], the dispersion relation Eq. (18) and the nonlinear Schrödinger

Eq. (29) in Ref. [56] can be reduced to Eqs. (9) and (10) here, respectively. The electron density $\tilde{n}$, the longitudinal component $\tilde{u}$ of the electron velocity and electrostatic potential $\tilde{\phi}$ are $\tilde{n} \simeq 1+\frac{2\tilde{k}^2}{4\tilde{\omega}^2-1}(\tilde{A})^2$, $\tilde{u} \simeq \frac{2\tilde{k}\tilde{\omega}}{4\tilde{\omega}^2-1}(\tilde{A})^2$, and $\tilde{\phi} \simeq -\frac{1}{2(4\tilde{\omega}^2-1)}(\tilde{A})^2+\frac{1}{2}|\tilde{A}|^2$, respectively.[56] According to $\boldsymbol{E}=-\nabla\phi-\frac{\partial \boldsymbol{A}}{\partial t}$ and Eq. (7), the electric field $\tilde{\boldsymbol{E}}$ and $\tilde{p}_y$ are expressed as

$$\tilde{\boldsymbol{E}} = \tilde{E}_y\hat{y} \simeq -2\varepsilon\tilde{\omega}|\tilde{\psi}(x,t)|\sin(\tilde{k}\tilde{x}-\tilde{\omega}\tilde{t} +\Theta(\psi(x,t)))\hat{y}, \tag{13}$$

$$\tilde{p}_y = 2\varepsilon|\tilde{\psi}(x,t)|\cos(\tilde{k}\tilde{x}-\tilde{\omega}\tilde{t}+\Theta(\psi(x,t))), \tag{14}$$

where $|\tilde{\psi}(x,t)|$ and $\Theta(\psi(x,t))$ are respective the modulus and amplitude angle of $\psi(x,t)$. From these results, it is noted that only the electric field $\tilde{\boldsymbol{E}}$ and transverse electrons momentum $\tilde{p}_y$ are first-order parameters, while the electron density $\tilde{n}$, longitudinal electrons velocity $\tilde{u}$ and electrostatic potential $\tilde{\phi}$ are second-order parameters, so we mainly observe the electric field $\tilde{\boldsymbol{E}}$ and transverse electrons momentum $\tilde{p}_y$ in the following discussion. In Eqs. (13) and (14), $2\varepsilon|\tilde{\psi}(x,t)| \ll 1$ is restricted by the weak relativistic condition $\tilde{A} \ll 1$.

2.2. Envelope EM solitary wave

The propagation of EM waves in plasmas requires $\tilde{\omega} > 1$, which means $D/N > 0$. Thus, Eq. (10) admits the bright envelope solitary wave solution[83] $\tilde{\psi} = \tilde{\rho}_0\mathrm{sech}(\frac{\tilde{\eta}-\tilde{U}_s\tilde{\tau}}{\tilde{W}})\mathrm{e}^{\mathrm{i}(\frac{1}{2D}[\tilde{\eta}\tilde{U}_s-(DN\tilde{\rho}_0^2+\frac{1}{2}\tilde{U}_s^2)\tilde{\tau}])}$, where $\tilde{U}_s$ represents the constant velocity of the bright solitary wave in coordinates (η,τ), and width $\tilde{W}$ is inversely proportional to the amplitude $\tilde{\rho}_0$ as $\tilde{W}\tilde{\rho}_0 = (2D(\tilde{\omega})/N(\tilde{\omega}))^{1/2} =$ constant. Setting $\tilde{a}_0 = 2\varepsilon\tilde{\rho}_0$, $\tilde{u}_s = \varepsilon\tilde{U}_s$, and using Eqs. (13) and (14), $\tilde{E}_y$ and $\tilde{p}_y$ can be written as follows:

$$\tilde{E}_y = -\tilde{E}_0\mathrm{sech}\left[\frac{\tilde{x}-(\tilde{v}_g+\tilde{u}_s)\tilde{t}}{\tilde{r}_0}\right]\sin\left[\tilde{k}\tilde{x}-\tilde{\omega}\tilde{t} +\frac{1}{2D}\left[\tilde{u}_s(\tilde{x}-\tilde{v}_g\tilde{t})-\left(\frac{1}{4}DN\tilde{a}_0^2+\frac{1}{2}\tilde{u}_s^2\right)\tilde{t}\right]\right], \tag{15}$$

$$\tilde{p}_y = \tilde{a}_0\mathrm{sech}\left[\frac{\tilde{x}-(\tilde{v}_g+\tilde{u}_s)\tilde{t}}{\tilde{r}_0}\right]\cos\left[\tilde{k}\tilde{x}-\tilde{\omega}\tilde{t} +\frac{1}{2D}\left[\tilde{u}_s(\tilde{x}-\tilde{v}_g\tilde{t})-\left(\frac{1}{4}DN\tilde{a}_0^2+\frac{1}{2}\tilde{u}_s^2\right)\tilde{t}\right]\right], \tag{16}$$

where $\tilde{E}_0 = \tilde{a}_0\tilde{\omega}$ is the amplitude of the electric field, $\tilde{a}_0 \ll 1$ is the amplitude of the dimensionless vector potential $\tilde{A}$ (restricted by the weak relativistic condition $\tilde{A} \ll 1$), $\tilde{v}_g+\tilde{u}_s$ represents the velocity of the solitary waves with $\tilde{u}_s \ll 1$, $\tilde{r}_0 = 2\sqrt{2D(\tilde{\omega})/N(\tilde{\omega})}/\tilde{a}_0$ represents the width of the envelope solitary waves, and the amplitudes and width satisfy $\tilde{E}_0\tilde{r}_0 = 2\tilde{\omega}\sqrt{2D(\tilde{\omega})/N(\tilde{\omega})} =$ constant, $\tilde{a}_0\tilde{r}_0 = 2\sqrt{2D(\tilde{\omega})/N(\tilde{\omega})} =$ constant for a given $\tilde{\omega}$. As can be seen from Eqs. (15) and (16), the envelope solitary wave structures for the electric field $\tilde{E}_y$ and the transverse electron momentum $\tilde{p}_y$ have the same constant velocity $\tilde{v}_g+\tilde{u}_s$, the same wave width $\tilde{r}_0$, but differ in the phase by $\pi/2$.

2.3. Modulational instability

Equation (10) supports an exact plane wave solution which gives the following electric field $\tilde{E}_y$,

$$\tilde{E}_y = -\tilde{E}_0\sin\left(\tilde{k}\tilde{x}-\tilde{\omega}\tilde{t}+\frac{1}{4}N\tilde{a}_0^2\tilde{t}\right), \tag{17}$$

where $\tilde{E}_0 = \tilde{a}_0\tilde{\omega}$. To study the linear stability of the plane wave, a small perturbation[84] (with a frequency $\tilde{\Omega} \ll \tilde{\omega}$, and a wavenumber $\tilde{K} \ll \tilde{k}$) leads to a dispersion relation of the form $\tilde{\Omega}^2 = D^2\tilde{K}^2(\tilde{K}^2-2\frac{N}{D}\tilde{a}_0^2)$. From this nonlinear dispersion relation, it is found that the modulational instability occurs when $\tilde{K}$ is in the range of

$$0 < |\tilde{K}| < \tilde{K}_c = \tilde{a}_0\sqrt{2N(\tilde{\omega})/D(\tilde{\omega})}, \tag{18}$$

where $\tilde{K}_c$ represents the maximum critical wavenumber of the modulational instability, and the corresponding growth rate for $\tilde{K}$ is

$$\tilde{\Gamma} = D(\tilde{\omega})\tilde{K}(2\frac{N(\tilde{\omega})}{D(\tilde{\omega})}\tilde{a}_0^2-\tilde{K}^2)^{1/2}. \tag{19}$$

The modulational instability growth rate attains a maximum

$$\tilde{\Gamma}_{\max} = \tilde{a}_0^2N(\tilde{\omega}) \tag{20}$$

for $\tilde{K} = \tilde{K}_{\Gamma\max} = \tilde{a}_0\sqrt{N(\tilde{\omega})/D(\tilde{\omega})}$ the most probable wave number. The dependence of $\tilde{K}_c$ and $\tilde{\Gamma}_{\max}$ on $\tilde{a}_0$ and $\tilde{\omega}$ is shown in Fig. 1. These theoretical results of modulational instability are calculated and represented by observable parameters in PIC simulation here.

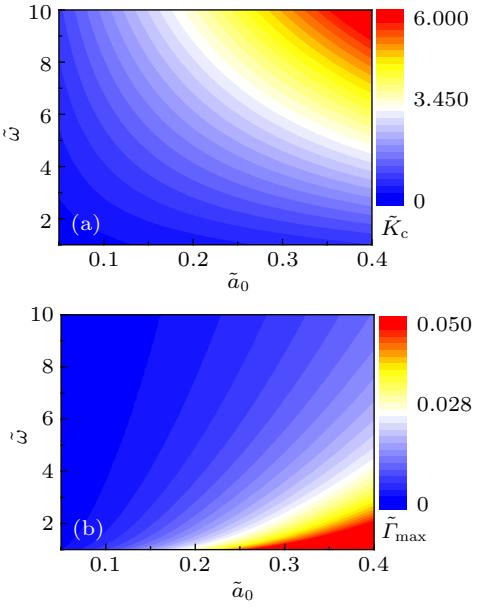


Fig. 1. The dependence of the maximum critical wave number $\tilde{K}_c$ (a) and the maximum growth rate $\tilde{\Gamma}_{\max}$ (b) of the modulational instability on $\tilde{a}_0$ and $\tilde{\omega}$.

3. Propagation dynamics and stability of EM solitary wave by PIC simulation

The propagation dynamics and stability of EM solitary wave will be investigated by 1D PIC simulation based on the above theoretical model here. The total length of the x direction is $L_x = 35\lambda_0$, where $\lambda_0 = 2\pi c/\omega$ is the wavelength of the carrier. The grid step is $\Delta x = 0.02\lambda_0$, and the time step is $\Delta t = 0.003T_0$ with $T_0 = 2\pi/\omega$ the period of the carrier wave. The macro-particles are uniformly distributed in the whole simulation region. In the initial period of time, an oscillating electric field is applied at the left boundary to excite the EM pulse. After the EM pulse moves to the center of the calculation window, a moving window is used in the propagation direction to save computation time and to avoid the reflection of EM wave at the boundary. All the physical parameters in our PIC simulation program are in International System of Units, and the basic physical parameters conversion relations are listed in Eq. (6), based on which the parameters of solitary waves and modulational instability are $E_0 = \tilde{E}_0 \frac{m_0 c\omega_{pe}}{e}$, $a_0 = \tilde{a}_0 \frac{mc^2}{e}$, $r = \tilde{r}_0 \frac{c}{\omega_{pe}}$, $v = (\tilde{v}_g + \tilde{u}_s)c$, $K = \tilde{K}k_{pe}$, and $\Gamma = \tilde{\Gamma}\omega_{pe}$ here.

Now, we study the propagation dynamics of EM solitary wave and verify the correctness of the theory. To excite a solitary wave like Eq. (15), we add an oscillating electric field at $x = 0$ (the left boundary) as follows:

$$E_y = \tilde{E}_0 \frac{mc\omega_{pe}}{e} \mathrm{sech}\left[\frac{-(\tilde{v}_g + \tilde{u}_s)c\omega_{pe}t}{\tilde{r}_0 c}\right] \times \sin\left[\left(\tilde{\omega} + \frac{1}{2D}\tilde{u}_s\tilde{v}_g + \frac{1}{8}N\tilde{a}_0^2 + \frac{1}{4D}\tilde{u}_s^2\right)\omega_{pe}t\right], \quad (21)$$

where $\tilde{E}_0 = \tilde{a}_0\tilde{\omega}$ is the initial amplitude of the oscillating electric field. By changing the amplitude $\tilde{E}_0$ at $x = 0$, one can control the shape of the excited wave. Thus the solitary wave can be investigated for different $\tilde{a}_0$ or $\tilde{\omega}$ clearly. In the following calculation, we set $\tilde{u}_s = 0.006$ in Eq. (21) and adopt the plasma density $n_e = 1 \times 10^{23}$ m^{-3}.

Through 1D PIC simulation, it is found that the excited EM solitary wave can propagate stably in a long time, in which the shape and the group velocity of the solitary wave do not change. After this period of time, the solitary wave begins to deform and become unstable. An example is shown in Fig. 2, where the stable propagation of the solitary wave and the instability after $x \approx 30.5$ mm are well displayed. In the following, we mainly investigate the stable motion characteristics in comparison with the theoretical prediction and the instability of the solitary wave.

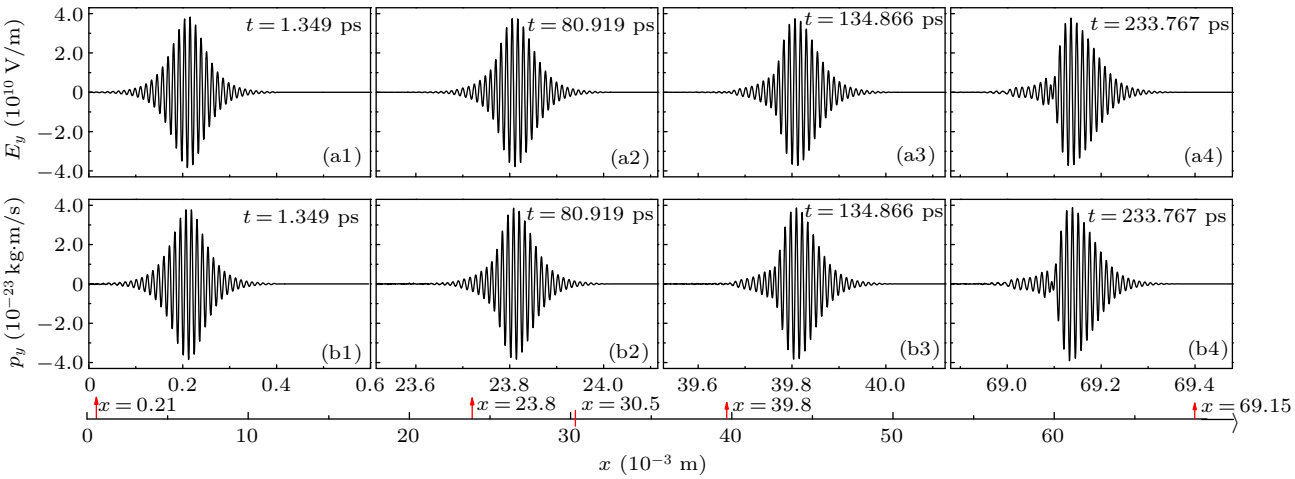


Fig. 2. The PIC simulation results of the evolution of solitary wave at different times. The boundary condition is given by Eq. (21) with $\tilde{\omega} = 7.0$ (the frequency ω is about 1.25×10^{14} s^{-1}), $\tilde{a}_0 = 0.18$ (the peak intensity I is about 1.95×10^{14} W/cm^2). Here (a1)–(a4) and (b1)–(b4) display the electric field E_y and transverse electron momentum p_y.

Figure 3 shows the PIC simulation results (black rhombuses) of the motion characteristics of the EM solitary wave compared with the theoretical results (blue lines) before instability occurs. Dependences of the electric field amplitude $\tilde{E}_0$, width $\tilde{r}_0$, and the group velocity $\tilde{v}$ of the solitary wave on the frequency $\tilde{\omega}$ and the dimensionless vector potential amplitude $\tilde{a}_0$ are shown in the two columns of Fig. 3. It is observed that the amplitude $\tilde{E}_0$ and width $\tilde{r}_0$ are in good agreement with the theoretical results for different solitary wave shapes. The velocities are also consistent with those shown in Eq. (15) except a slight reduction for the larger $\tilde{\omega}$.

To investigate the instability of the solitary wave, the propagation distance L before the laser becomes unstable is measured. The distance L versus the frequency $\tilde{\omega}$ and the dimensionless vector potential amplitude $\tilde{a}_0$ is shown in Figs. 4(a) and (b). From Fig. 4(a), it can be seen that there exists a catastrophe point at $\tilde{\omega} \simeq 3.83$. The distance L is very long for $\tilde{\omega} < 3.83$, but suddenly drops by two orders of magnitude when $\tilde{\omega} \simeq 3.83$ and begins to increase with the further increase of $\tilde{\omega}$. Figure 4(b) shows that L decreases with the increase of $\tilde{a}_0$, which means that the solitary wave becomes more unstable as $\tilde{a}_0$ increases. In Fig. 4(a), the frequencies of

the EM wave are respectively $\tilde{\omega} = 2.0, 2.5, 3.0, 3.5, 3.8, 3.85, 4.0, 4.5, 5.0, 5.5, 6.0, 6.5, 7.0, 8.0$. The corresponding dispersion coefficient D and the nonlinear coefficient N are, respectively, $D = 0.0625$, $N = 0.325$; 0.032, 0.265; 0.0185, 0.2246; 0.0117, 0.1951; 0.0091, 0.1810; 0.0088, 01788; 0.0078, 0.726; 0.0055, 0.1548; 0.0040, 0.1403; 0.0030, 0.1283; 0.0023, 0.1182; 0.0018, 0.1096; 0.0016, 0.1021; 0.0010, 0.0899. In Fig. 4(b), $\tilde{\omega} = 6.0$, $D = 0.0023$, $N = 0.1182$.

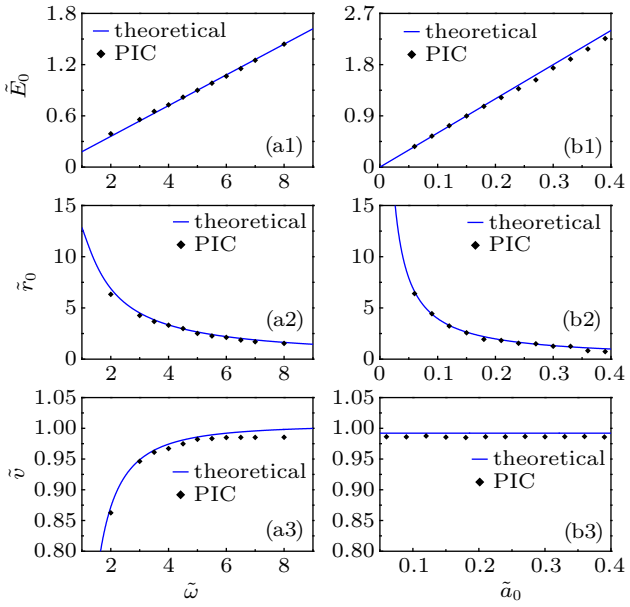


Fig. 3. The comparison between the theoretical results given by Eq. (15) and the PIC numerical ones of the solitary wave. The dependences of the amplitude, width, and velocity of the solitary wave on $\tilde{\omega}$ and $\tilde{a}_0$ are shown in (a1)–(a3) and (b1)–(b3); $\tilde{a}_0 = 0.18$ in (a1)–(a3), $\tilde{\omega} = 6.0(1.07 \times 10^{14}\ \mathrm{s}^{-1})$ in (b1)–(b3). In (a1)–(a3), the range of the frequency $\tilde{\omega}$ is $2\omega_{pe} - 8\omega_{pe}$, and the corresponding specific value is about $3.57 \times 10^{13}\ \mathrm{s}^{-1} - 1.43 \times 10^{14}\ \mathrm{s}^{-1}$, the range of peak intensity is about $1.59 \times 10^{13}\ \mathrm{W/cm^2} - 2.55 \times 10^{14}\ \mathrm{W/cm^2}$. In (b1)–(b3), the range of the dimensionless vector potential amplitude $\tilde{a}_0$ is 0.06–0.39, the corresponding range of peak intensity is about $1.59 \times 10^{13}\ \mathrm{W/cm^2} - 6.72 \times 10^{14}\ \mathrm{W/cm^2}$. The input envelope is actually the shape of the EM solitary wave with a wave width of about 17 μm–110 μm.

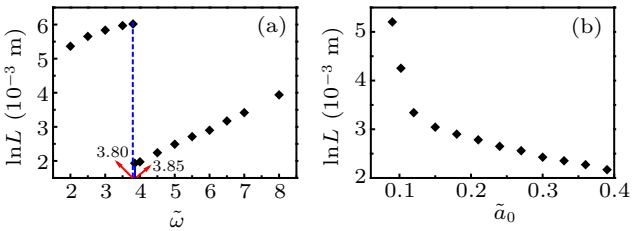


Fig. 4. The dependence of the natural logarithm of distance L on $\tilde{\omega}$ (a) and $\tilde{a}_0$ (b); $\tilde{a}_0 = 0.18$ in (a), $\tilde{\omega} = 6.0$ in (b). The laser frequency and the peak intensity in (a) are corresponding to Figs. 3(a1)–3(a3), and in (b) are corresponding to Figs. 3(b1)–3(b3).

To show the comparison of propagation between PIC simulation and theoretical results clearly and understand the above instability phenomena, it is necessary to display the process of solitary wave evolution under different parameters. Figure 5 shows the evolution of the excited solitary wave with different $\tilde{\omega}$ for $\tilde{a}_0 = 0.18$. From Figs. 5(a1)–5(a2), 5(a5)–5(a6), and (a9)–(a10), we can see that the shapes of the excited (black line) EM solitary waves are in good agreement with the theoretical results (blue dashed line) of Eq. (15) in the stable propagation stage for different $\tilde{\omega}$. Meanwhile, the PIC simulation results lag behind the theoretical ones, which means that the velocity of the excited solitary wave is slightly smaller than that of Eq. (15). With the increase of $\tilde{\omega}$, the lag phenomenon appears earlier. Now we pay attention to the instability of solitary waves. It can be obviously seen from Figs. 5(a3)–5(a4), (a7)–5(a8), and (a11)–(a12) that the stable propagation distance of solitary wave for $\tilde{\omega} = 2.0$ is much longer than others, and the instability in Fig. 5(i) is quite different from those in Figs. 5(ii) and 5(iii). It seems that the instability in Fig. 5(i) is related to the calculation errors in PIC simulation (we have verified this point by higher resolution simulations in space and time, and found that the stable propagation distance will increase at a higher resolution in space and time), while the deformations in Figs. 5(ii) and 5(iii) are due to the real physical instability in the interaction between the EM solitary waves and plasmas. For understanding the real physical instability in Figs. 5(ii) and 5(iii), we measured the instability space periods λ_{in} and found $\lambda_{in} \simeq 110 \times 10^{-6}$ m in Fig. 5(ii) and $\lambda_{in} \simeq 102 \times 10^{-6}$ m in Fig. 5(iii), which just respectively fall in the theoretical wavelength ranges of modulational instability $\lambda > 58.05 \times 10^{-6}$ m for Fig. 5(ii) and $\lambda > 43.23 \times 10^{-6}$ m for Fig. 5(iii) calculated by Eq. (18). For other values of $\tilde{\omega} \geq 3.83$ shown in Fig. 4(a), the similar instability space periods and deformations are also found. Thus we think that the deformations in Figs. 5(ii) and 5(iii) may be caused by the modulational instability. Moreover, the fact that the increase of L with $\tilde{\omega} > 3.83$ displayed in Figs. 4(a), 5(a7), and 5(a11) is consistent with that shown by the modulational instability growth rate Eq. (19), i.e., the growth rate $\tilde{\Gamma}$ decreases with the increase of $\tilde{\omega}$ (see Fig. 1(b)). In a word, after stable propagation over a long distance, the occurrence of modulational instability causes the deformation of the solitary wave for $\tilde{\omega} \geq 3.83$. Increasing $\tilde{\omega}$ can reduce the growth rate $\tilde{\Gamma}$ of modulational instability and delay the wave deformation, thereby allows the EM wave to stably propagate for longer distance. Why modulational instability does not observe for $\tilde{\omega} < 3.83$. We think that, in addition to its own very small instability growth rate, the key is related to the slight disturbance of the EM wave in the interaction between the EM solitary wave and plasmas. To demonstrate this, the longitudinal electronic momentum p_x at $t = 20$ ps long before the occurrence of the instability for different $\tilde{\omega}$ are shown in Figs. 6(a1)–6(a3), associating with the corresponding electric field E_y in Figs. 6(b1)–(b3) for comparison. It can be seen from Figs. 6(a1) and 6(b1) that the profile of p_x is basically the same as that of the EM solitary wave, which means that the plasma nearly does not disturb the profile of the EM solitary wave for $\tilde{\omega} = 2.0$. For $\tilde{\omega} = 6.0$ and

8.0, however, Figs. 6(a2)–6(b2) and 6(a3)–6(b3) show that, around and behind the "hillsides" marked by the red dashed lines, there are relatively obvious inconsistencies between the distributions of p_x and the EM solitary waves, which then give disturbances to the EM solitary waves and induce the modulational instability. In Figs. 5(ii) and 5(iii), the initial deformations of the EM solitary waves are just around the "hillsides" of the EM solitary waves and this confirms the role of the disturbances for modulational instability. Figure 7 shows the evolution of the excited envelope solitary waves with different $\tilde{a}_0$ for $\tilde{\omega} = 6.0$. From Figs. 7(a1)–7(a2), (a5)–(a6), and (a9)–(a10), we can see that the shapes of the excited (black line) EM solitary waves are in good agreement with the theoretical results (blue dashed line) of Eq. (15) in the stable propagation stage for different $\tilde{a}_0$. Compared with the theoretical results, the lag phenomenon is also observed. It can be seen from Figs. 7(a3)–7(a4), 7(a7)–7(a8), 7(a11)–7(a12), and 6(a4)–6(b4), 6(a5)–6(b5), 6(a6)–6(b6) that the deformations of the EM solitary waves here are due to modulational instability. Since the growth rate $\tilde{\Gamma}$ increases with the increase of $\tilde{a}_0$, the stable propagation distance L decreases with the increase of $\tilde{a}_0$ as displayed in Fig. 4(b).

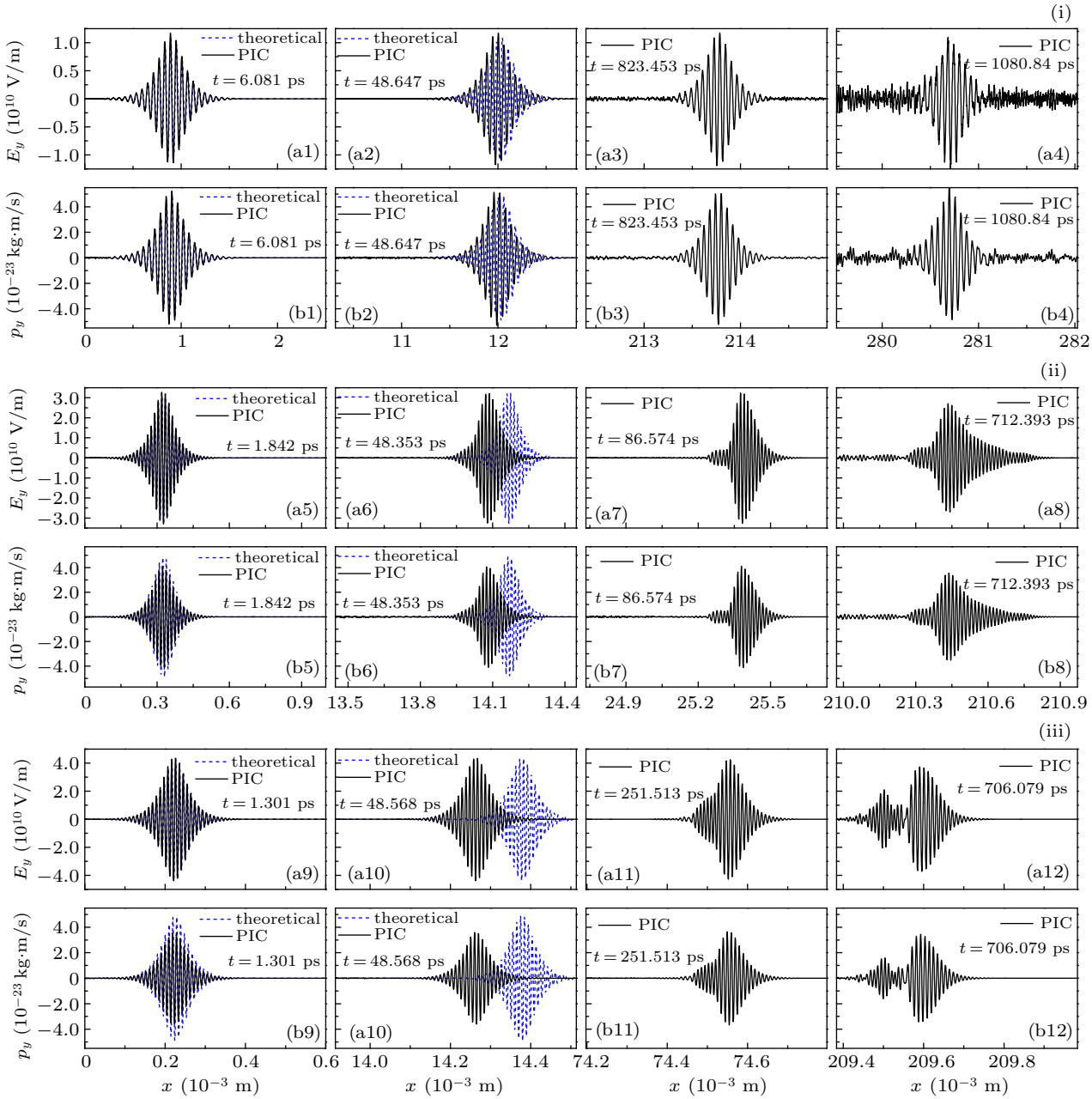


Fig. 5. The evolution of the excited solitary wave with $\tilde{\omega} = 2.0$ (i), 6.0 (ii), and 8.0 (iii) for $\tilde{a}_0 = 0.18$. The peak intensities I of the solitary waves are respectively 1.59×10^{13} W/cm^2 (i), 1.43×10^{14} W/cm^2 (ii) and 2.55×10^{14} W/cm^2 (iii). The frequencies ω are respectively about 3.57×10^{13} s^{-1} (i), 1.07×10^{14} s^{-1} (ii) and 1.43×10^{14} s^{-1} (iii). Here (a1)–(a12) and (b1)–(b12) display the electric fields E_y and transverse electron momentums p_y at different times. The theoretical results of the electric field Eq. (15) and the transverse electron momentum Eq. (16) are only shown in the stable propagation stage.

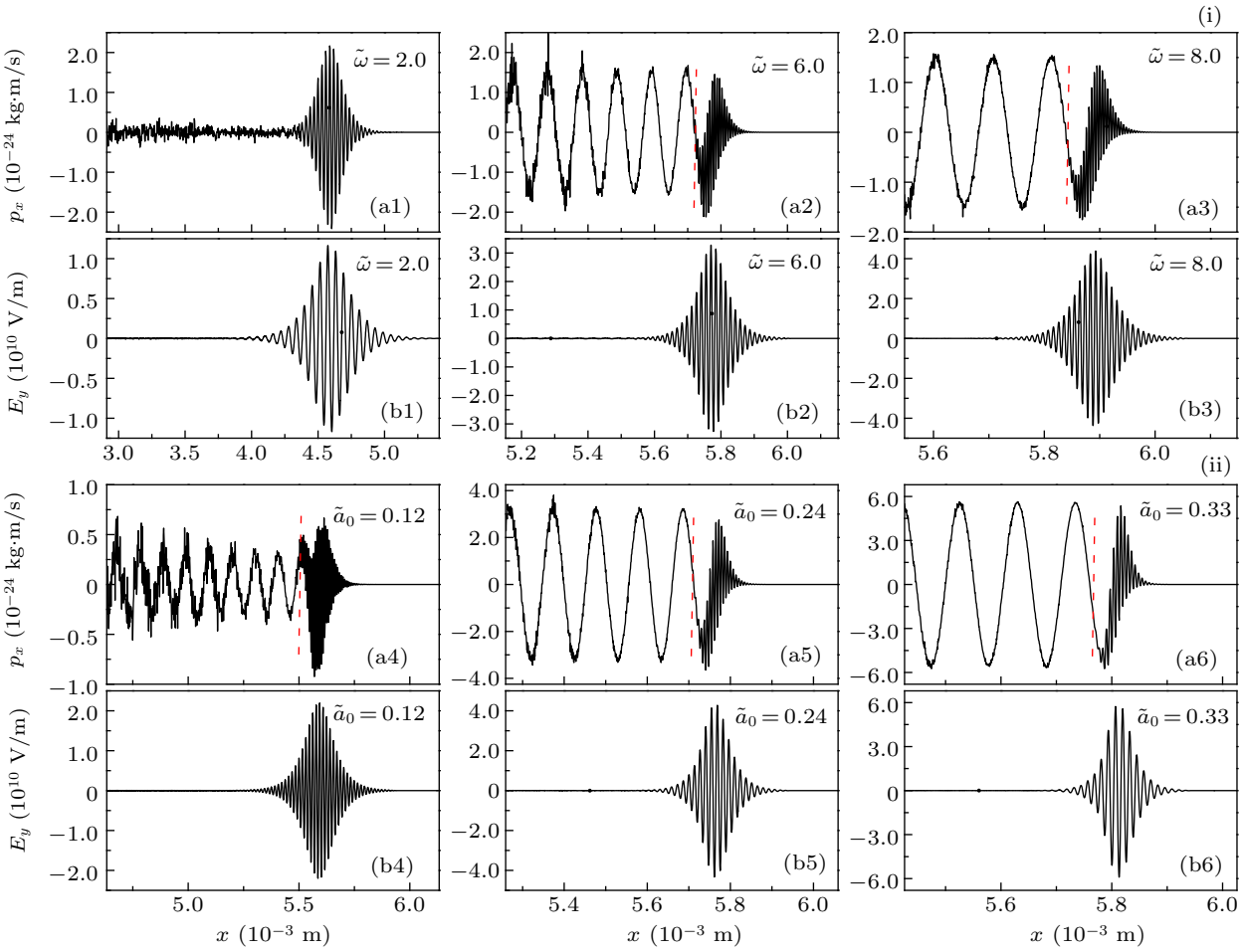


Fig. 6. PIC simulation results of the longitudinal electronic momentum p_x and the corresponding electric field E_y at $t = 20$ ps long before the occurrence of the instability. Here upper six panels (i) show these parameters with different $\tilde{\omega}$ for $\tilde{a}_0 = 0.18$; and lower six panels (ii) with different $\tilde{a}_0$ for $\tilde{\omega} = 6.0$.

From Figs. 5 and 7, it is found that the evolution of the excited (black line) transverse electron momentum $\tilde{p}_y$ is synchronous with the evolution of the EM solitary waves. That is to say, it experiences the same long-distance stable propagation and becomes unstable at the same time and position. It is also noted that for the small $\tilde{\omega}$ and $\tilde{a}_0$ (Figs. 5(i) and 7(i)), the amplitudes of $\tilde{p}_y$ are basically consistent with the theoretical results (blue line) of Eq. (16), but for the large $\tilde{\omega}$ and $\tilde{a}_0$ (Figs. 5(ii)–5(iii) and Figs. 7(ii)–7(iii)), the amplitudes of $\tilde{p}_y$ are slightly smaller than the theoretical ones.

From Fig. 6, it is found that the EM solitary wave may excite the wakefield. We measured the oscillation frequency ω_{we} of the electron in the wakefield and found $\omega_{we} \simeq 1.7894 \times 10^{13}$ s^{-1} in Figs. 6(a2)–6(a6). Noting the plasma frequency $\omega_{pe} = 1.7840 \times 10^{13}$ s^{-1} and the cold plasmas here, we think that the wakefield is a Langmuir oscillation. Detailed simulation indicates that, for $n_e = 1 \times 10^{23}$ m^{-3} and $\tilde{a}_0 = 0.18$, the Langmuir oscillation is only excited when the frequency $\tilde{\omega} \geq 3.83$ (Figs. 6(a2) and (a3)), while the wakefield is not obvious when $\tilde{\omega} < 3.83$ (such as Fig. 6(a1) for $\tilde{\omega} = 2.0$). The frequency of Langmuir oscillation has nothing to do with $\tilde{\omega}$ and $\tilde{a}_0$, but only is related to the plasma background (plasma density). The amplitude of Langmuir oscillation changes slightly with the increase of $\tilde{\omega}$ but obviously increases with the increase of $\tilde{a}_0$.

Finally, it will be seen in the next section that Langmuir oscillation plays the key modulational role in the modulational instability of plane EM wave. With noting the "hillsides" corresponding to the excitation positions of Langmuir oscillation in Fig. 6 and the wavelength of modulation by Langmuir oscillation $2\pi c/\omega_{pe} \simeq 105.7 \times 10^{-6}$ m approximately identical to the measured instability space periods $\lambda_{in} \simeq 110 \times 10^{-6}$ m in Fig. 5(ii) and $\lambda_{in} \simeq 102 \times 10^{-6}$ m in Fig. 5(iii), we can also directly say that the excited Langmuir oscillation plays an important modulational role here and induces the instability of EM solitary wave finally. The sudden variation of L around $\tilde{\omega} \simeq 3.83$ in Fig. 4(a) is due to the excitation of Langmuir oscillation.

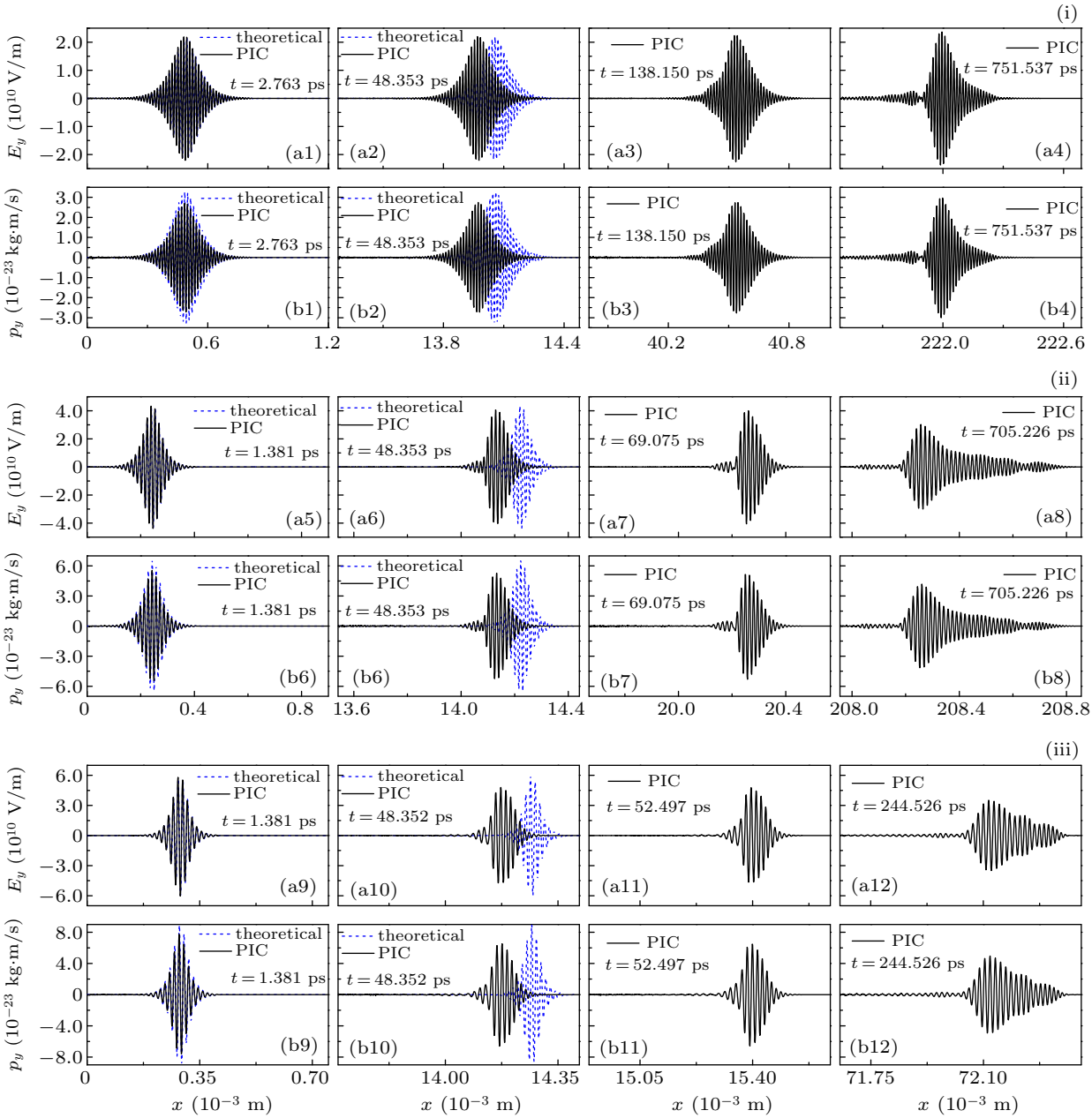


Fig. 7. The evolution of the excited solitary wave with $\tilde{a}_0 = 0.12$ (i), 0.24 (ii), and 0.33 (iii) for $\tilde{\omega} = 6.0$ (1.07×10^{14} s^{-1}). The peak intensities I of the solitary waves are respectively about 6.36×10^{13} W/cm^2 (i), 2.55×10^{14} W/cm^2 (ii), and 4.81×10^{14} W/cm^2 (iii). Here (a1)–(a12) and (b1)–(b12) display the electric fields E_y and transverse electron momentums p_y at different times. The theoretical results of the electric field Eq. (15) and the transverse electron momentum Eq. (16) are only shown in the stable propagation stage.

4. PIC simulation of modulational instability

In this section, the modulational instability of plane EM wave is studied by 1D PIC simulation. The total length of x direction is $L_x = 152\lambda_0$, the grid step is $\Delta x = 0.07\lambda_0$, and the time step is $\Delta t = 0.002T_0$. To excite a plane EM wave, we add an oscillating electric field at $x = 0$ (the left boundary) as follows:

$$E_y = \tilde{E}_0 \frac{mc\omega_{\rm pe}}{e} \sin\left(\tilde{\omega}\omega_{\rm pe}t - \frac{1}{4}N\tilde{a}_0^2\omega_{\rm pe}t\right) \times \begin{cases} \sin(\alpha t), & 0 < t < t_1, \\ 1, & t_1 < t < t_2, \\ \sin[\frac{\pi}{2} + \alpha(t - t_2)], & t_2 < t < t_1 + t_2, \end{cases} \quad (22)$$

where $\alpha = \frac{\pi}{2}/t_1$, $t_1 = 0.85$ ps, $t_2 = 10$ ps. In Eq. (22), the time from $0 < t < t_1$ corresponds to the excitation of the rising edge, the time from $t_1 < t < t_2$ corresponds to the excitation of the plane wave with constant amplitude, and the time from $t_2 < t < t_1 + t_2$ corresponds to the excitation of the falling edge. The plasma density is $n_{\rm e} = 0.2 \times 10^{23}$ m^{-3}.

To get a knowledge of the occurrence and evolution of the modulational instability, the evolution of the plane EM wave with $\tilde{a}_0 = 0.12$ and $\tilde{\omega} = 6.0$ is plotted in Fig. 8. It can be seen from Fig. 8(a2) that a ripple with equal intervals appears with the evolution of time, which indicates the occurrence of instability. The ripple depth gradually deepens from the front of the plane wave to the back. With the further

evolution of time, Fig. 8(a3) shows that the instability continues to develop, and the instability at the back of the plane wave grows faster than that at the front. The wave number of the instability can be measured from Figs. 8(b1)–8(b3) of the wave number spectra. The highest peak in Figs. 8(b1)–8(b3) corresponds to $k = 159.1$ mm^{-1} of the carrier wave. From Fig. 8(b2), we can see that the corresponding instability wave number $K \simeq (187.3 - 159.1)$ mm^{-1} $\simeq (159.1 - 130.8)$ mm^{-1} $\simeq 28.2$ mm^{-1}. After a period time of the instability evolution, it is noted from Fig. 8(b3) that the proportion of this wave number increases significantly, and a new component of $(159.1 - 102.6)$ mm^{-1} $\simeq 56.5$ mm^{-1} $\simeq 2$ K appears. With the instability development, higher-time components appear one after another, and are not further displayed here. The wave number range for modulational instability obtained by theoretical analysis is $(0, K_c \simeq 32.3$ mm$^{-1})$ and this wave number $K \simeq 28.2$ mm^{-1} is just in it. To investigate the speed of the instability development, we measured the instability growth rate at the front, middle and back of the plane wave, and found that $\Gamma_{\text{front}} \simeq 1.48 \times 10^{-2}/$ ps, $\Gamma_{\text{middle}} \simeq 2.50 \times 10^{-2}/$ ps, and $\Gamma_{\text{back}} \simeq 3.49 \times 10^{-2}/$ ps. The reason for $\Gamma_{\text{back}} > \Gamma_{\text{middle}} > \Gamma_{\text{front}}$ is that the local plasma interacting with the middle part of the plane electromagnetic wave has already experienced a continuous disturbance by the first half of the wave train for a time $(t_2 - t_1)/2$, and similarly, the local plasma interacting with the back part of the plane electromagnetic wave has already experienced a continuous disturbance by the full wave train for a time $t_2 - t_1$. Because of the same reason, we think that Γ_{front} is more in line with the condition of theoretical analysis in subsection 2.3. Equation (19) tells us that the theoretical growth rate for $K \simeq 28.2$ mm^{-1} is $\Gamma_{\text{theoretical}} \simeq 1.202 \times 10^{-2}/$ ps. Considering $K \simeq 28.2$ mm^{-1} $\in (0, K_c \simeq 32.3$ mm$^{-1})$ and $\Gamma_{\text{front}} \simeq \Gamma_{\text{theoretical}}$, we think that the observed instability in Fig. 8 is the modulational instability. This also confirms the theory of the modulational instability.

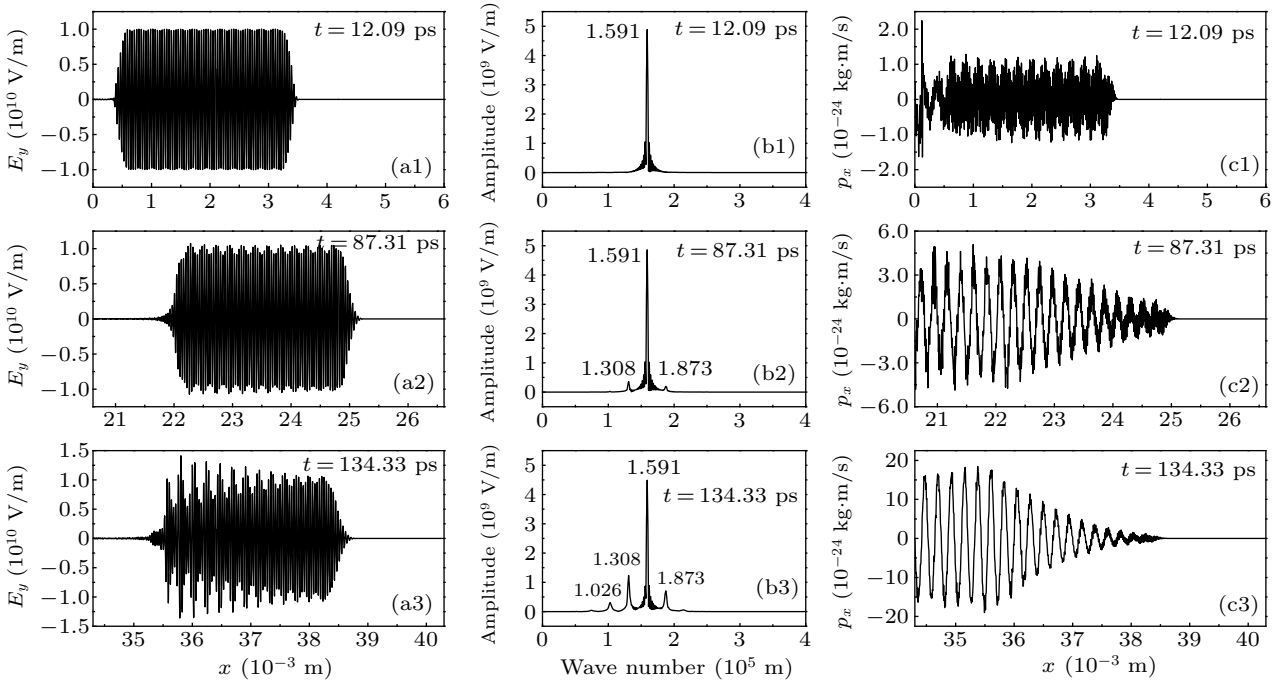


Fig. 8. The PIC simulation results of the evolution of plane wave at different times. The boundary condition is given by Eq. (22) with $\tilde{a}_0 = 0.12$ (the intensity I of the plane wave is about 1.27×10^{13} W/cm^2) and $\tilde{\omega} = 6.0$ (the frequency ω is about 4.78×10^{13} s^{-1}). Here (a1)–(a3) display the electric field E_y of the plane wave, (b1)–(b3) illustrate the wave number spectra of (a1)–(a3) by FFT, and (c1)–(c3) show the longitudinal momentum p_x corresponding to (a1)–(a3).

To investigate the influence of the carrier wave frequency $\tilde{\omega}$ and the dimensionless vector potential amplitude $\tilde{a}_0$ on modulational instability and further check the instability theory, we give the wave numbers K of the instability and the corresponding growth rate Γ for different $\tilde{\omega}$ and $\tilde{a}_0$ in Fig. 9. The observed wave numbers K of the modulational instability in PIC simulation are indicated by black rhombus in Figs. 9(a1) and 9(a2). The maximum critical wave number K_c for the instability occurrence and the most probable wave number $K_{\Gamma\max}$ obtained by theoretical analysis are also plotted by the blue dashed line and the blue line, respectively. It can be seen that the observed wave numbers are just in the theoretical wave number range of modulational instability, i.e., $K < K_c$. An interesting finding is that the observed wave numbers seem to have nothing to do with the most probable wave numbers and are closely around a value $K \simeq 27.9$ mm^{-1}, independent of $\tilde{\omega}$ and $\tilde{a}_0$. We think that the reason is related to Langmuir oscillation caused by the EM wave. The excited Langmuir oscillation gives a continuous modulation to the EM wave and then induces the modulational instability. The spatial wave

number of the modulation by Langmuir oscillation can be estimated to be $\omega_{pe}/c \simeq 27.3$ mm^{-1}, which is just consistent with the observed wave number $K \simeq 27.9$ mm^{-1} of the instability. To verify this point further, we measured the wave numbers K of the instability under other plasma frequencies, which are found to be also approximately equal to ω_{pe}/c. The Langmuir oscillation of p_x just like Figs. 8(c1)–8(c3) is also observed. This confirms the correctness of the explanation and reveals the role of the modulation by Langmuir oscillation in the instability. The growth rate Γ of the modulational instability depending on the frequency $\tilde{\omega}$ and the dimensionless vector potential amplitude $\tilde{a}_0$ is shown in Figs. 9(b1) and 9(b2). It can be found from Fig. 9(b1) that the growth rate Γ of the instability slowly decreases with the increase of $\tilde{\omega}$. From Fig. 9(b2), we can see that the growth rate Γ increases with the increase of $\tilde{a}_0$, which means that the EM wave becomes more unstable as $\tilde{a}_0$ increases. Comparing Fig. 9(b1) with (b2), we find that the change of instability growth rate Γ with $\tilde{a}_0$ is more obvious than that with $\tilde{\omega}$, so the main factor influencing the modulational instability growth rate is $\tilde{a}_0$. Finally, Fig. 9 shows that the measured instability growth rate Γ is basically consistent with the theoretical value within the error range, which once again confirms the correctness of the theory of the modulational instability.

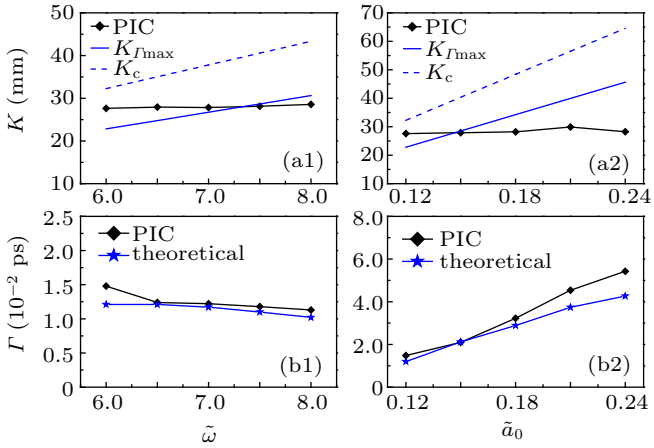


Fig. 9. The dependence of the observed wave number K and the corresponding instability growth rate Γ in PIC simulation on $\tilde{\omega}$ and $\tilde{a}_0$, for $\tilde{a}_0 = 0.12$ in (a1) and (b1), $\tilde{\omega} = 6.0(4.78 \times 10^{13}$ s$^{-1})$ in (a2) and (b2). The maximum critical wave number K_c of the modulational instability and the most probable wave number $K_{\Gamma\max}$ obtained by theoretical analysis are also plotted in (a1)–(a2). The theoretical growth rate $\Gamma_{\text{theoretical}}$ is also displayed in (b1) and (b2). In (a1) and (b1), the range of the frequency $\tilde{\omega}$ is $6\omega_{pe} - 8\omega_{pe}$ $(4.78 \times 10^{13}$ s$^{-1} - 6.38 \times 10^{13}$ s$^{-1})$, and the range of peak intensity is about 1.27×10^{13} W/cm^2 $- 2.26 \times 10^{14}$ W/cm^2. In (a2) and (b2), the range of the dimensionless vector potential amplitude $\tilde{a}_0$ is $0.12 - 0.24$, the corresponding range of peak intensity is about 1.27×10^{13} W/cm^2 $- 5.08 \times 10^{13}$ W/cm^2.

5. Conclusions

In summary, we have studied the propagation dynamics of EM solitary waves in uniform cold electron-ion plasmas by 1D PIC simulation. The EM solitary wave is excited by applying an oscillating electric field at the left boundary. It is found that the shape of the excited solitary wave, i.e., the amplitude and width, can remain unchanged and is identical to the theoretical profile in a long-distance stable propagation. The velocity is also consistent with the theoretical one except a very slight reduction for the larger carrier wave frequency. The instability study of the solitary wave indicates that, under the conditions of the plasma density $n_e = 1 \times 10^{23}$ m^{-3} and the dimensionless vector potential amplitude $\tilde{a}_0 = 0.18$, the solitary wave can stably propagate in the distance range of stable PIC calculation for the carrier wave frequency $\omega < 3.83\omega_{pe}$. However, for $\omega \geq 3.83\omega_{pe}$, the EM solitary wave deforms after a long enough distance. Further investigation shows that the deformation is closely related to the modulational instability and the wakefield excitation in the interaction between the solitary wave and the plasma. Concretely, the EM solitary wave may excite a weak Langmuir oscillation, which in turn modulates the EM solitary wave and thus induces modulational instability. For $\omega \geq 3.83\omega_{pe}$, the measured stable propagation distance of EM solitary wave increases with the increase of the carrier wave frequency and decreases with the increase of the dimensionless vector potential amplitude obviously. In these simulations, the transverse electron momentum also presents a solitary wave shape, and its evolution is fully synchronous with the EM solitary wave. In addition, about the catastrophe point $\omega \simeq 3.83\omega_{pe}$, there are some remaining problems, e.g., why is this value and how does this critical value relate to the physical background, which will be studied in our future work considering the corresponding workload.

Modulational instability is studied by exciting a plane EM wave. The simulation study shows that the observed spatial wave number of the modulational instability has nothing to do with the carrier wave frequency and the dimensionless vector potential amplitude, but is closely related to the plasma density and is approximately equal to the spatial modulated wave number of Langmuir oscillation. This obviously indicates that the occurrence of modulational instability is excited through the continues modulation of Langmuir oscillation induced by the EM wave itself. This also directly reveals the importance of the excitation of wakefield, i.e., the Langmuir oscillation, in the stable propagation of the EM wave. Observing a plane EM wave with instability, it can be found that the amplitude and the growth rate of the modulational instability become larger from the front to the back of the wave tain. The instability growth rate at the front of the wave is consistent with the theoretical value, which verifies the correctness of the theory of modulational instability. Further investigation shows that the dimensionless vector potential amplitude is the main factor affecting the modulational instability, and increasing it can significantly increases the growth rate of the modulational instability.

This study not only verifies the theory of EM solitary wave and modulational instability, but more importantly re-

ports the modulational instability of solitary wave for the first time, and reveals the importance of the excitation of Langmuir oscillation to the induction of modulational instability of EM wave, which has never been noticed before. Other main physical parameters influencing the stable propagation of EM waves are also illustrated. These results may also be important to the guidance of light, electron acceleration, wakefield generation and harmonic generation, etc.

References

[1] Mori W B, Decker C D and Leemans W P 1993 *IEEE Trans. Plasma Sci.* **21** 110

[2] Esarey E, Ting A, Sprangle P, Umstadter D and Liu X 1993 *IEEE Trans. Plasma Sci.* **21** 95

[3] Kuo C C, Pai C H, Lin M W, Lee K H, Lin J Y, Wang J and Chen S Y 2007 *Phys. Rev. Lett.* **98** 033901

[4] Niknam A R, Aliakbari A, Majedi S, Haji Mirzaei F and Hashemzadeh M 2011 *Phys. Plasmas* **18** 112305

[5] Bokaei B, Niknam A R and Milani M R J 2014 *Plasma Sources Sci. Technol.* **23** 064011

[6] Hashemzadeh M 2018 *Phys. Plasmas* **25** 012309

[7] Luo J, Chen M, Wu W Y, Weng S M, Sheng Z M, Schroeder C B, Jaroszynski D A, Esarey E, Leemans W P and Mori W B 2018 *Phys. Rev. Lett.* **120** 154801

[8] Razavinia S N and Ghorbanalilu M 2019 *Phys. Rev. Accel. Beams* **22** 111305

[9] Sprangle P, Joyce G, Esarey E and Ting A 1988 *AIP Conf. Proc.* **175** 231

[10] Tian J M, Tang R A, Hong X R, Yang Y, Wang L, Zhou W J and Xue J K 2016 *Phys. Plasmas* **23** 123117

[11] Zhang L, Tang R A, Hong X R, Gao J M, Yin L R, Tian J M, Cheng R J and Xue J K 2019 *Phys. Plasmas* **26** 043106

[12] Luo J, Chen M, Zeng M, Vieira J, Yu L, Weng S M, Silva L O, Jaroszynski D A, Sheng Z M and Zhang J 2016 *Sci. Rep.* **6** 29101

[13] Sprangle P, Esarey E and Ting A 1990 *Phys. Rev. A* **41** 4463

[14] Sharma A and Kourakis I 2010 *Plasma Phys. Controlled Fusion* **52** 065002

[15] Kozlov V A, Litvak A G and Suvorov E V 1979 *Zh. Eksp. Teor. Fiz.* **76** 148 [1979 *Sov. Phys. JETP* **49** 75]

[16] Farina D and Bulanov S V 2001 *Phys. Rev. Lett.* **86** 5289

[17] Hong X R, Xie B S, Zhang S, Wu H C and Zhao X Y 2011 *Phys. Plasmas* **18** 103106

[18] Zhang S, Xie B S, Hong X R, Wu H C and Zhao X Y 2011 *Phys. Plasmas* **18** 033104

[19] Xie B S and Hua C C 2005 *Commun. Theor. Phys.* **43** 1119

[20] Sen A and Kaw P K 1994 *Phys. Scripta* **T50** 47

[21] Weber S, Riconda C and Tikhonchuk V T 2005 *Phys. Rev. Lett.* **94** 055005

[22] Xiao C Z, Liu Z J, Wu D, Zheng C Y and He X T 2015 *Phys. Plasmas* **22** 052121

[23] Kaw P K, Sen A and Katsouleas T 1992 *Phys. Rev. Lett.* **68** 3172

[24] Liu S Q and Li X Q 2000 *Phys. Plasmas* **7** 3405

[25] Cheng L H, Tang R A, Zhang A X and Xue J K 2013 *Phys. Rev. E* **87** 025101

[26] Lehmann G, Laedke E W and Spatschek K H 2008 *Phys. Plasmas* **15** 072307

[27] Liu S Q, Tang W and Li X Q 2012 *Pramana-J. Phys.* **78** 439

[28] Esirkepov T, Nishihara K, Bulanov S V and Pegoraro F 2002 *Phys. Rev. Lett.* **89** 275002

[29] Bulanov S V, Esirkepov T Zh, Naumova N M, Pegoraro F and Vshivkov V A 1999 *Phys. Rev. Lett.* **82** 3440

[30] Borghesi M, Campbell D H, Schiavi A, Haines M G, Willi O, MacKinnon A J, Patel P, Gizzi L A, Galimberti M and Clarke R J 2002 *Phys. Plasmas* **9** 2214

[31] Borghesi M, Bulanov S, Campbell D H, Clarke R J, Esirkepov T Zh, Galimberti M, Gizzi L A, MacKinnon A J, Naumova N M and Pegoraro F 2002 *Phys. Rev. Lett.* **88** 135002

[32] Kartal S, Tsintsadze L N and Berezhiani V I 1996 *Phys. Rev. E* **53** 4225

[33] Mikaberidze G and Berezhiani V I 2015 *Phys. Lett. A* **379** 2730

[34] Poornakala S, Das A, Kaw P K, Sen A, Sheng Z M, Sentoku Y, Mima K and Nishikawa K 2002 *Phys. Plasmas* **9** 3802

[35] Lontano M, Passoni M and Bulanov S V 2003 *Phys. Plasmas* **10** 639

[36] Sánchez-Arriaga G, Siminos E and Lefebvre E 2011 *Phys. Plasmas* **18** 082304

[37] Verma D, Bera R K, Kumar A, Patel B and Das A 2017 *Phys. Plasmas* **24** 123111

[38] Sentoku Y, Esirkepov T Zh, Mima K, Nishihara K, Califano F, Pegoraro F, Sakagami H, Kitagawa Y, Naumova N M and Bulanov S V 1999 *Phys. Rev. Lett.* **83** 3434

[39] Naumova N M, Bulanov S V, Esirkepov T Zh, Farina D, Nishihara K, Pegoraro F, Ruhl H and Sakharov A S 2001 *Phys. Rev. Lett.* **87** 185004

[40] Liu Y, Klimo O, Esirkepov T Zh, Bulanov S V, Gu Y J, Weber S and Korn G 2015 *Phys. Plasmas* **22** 112302

[41] Sánchez-Arriaga G and Lefebvre E 2011 *Phys. Rev. E* **84** 036403

[42] Esirkepov T, Bulanov S V, Nishihara K and Tajima T 2004 *Phys. Rev. Lett.* **92** 255001

[43] Li B, Ishiguro S, Škorić M M, Song M and Sato T 2005 *Phys. Plasmas* **12** 103103

[44] Li B, Ishiguro S, Škorić M M and Sato T 2007 *Phys. Plasmas* **14** 032101

[45] Xie J Y, Deng Z H, Chang X and Tang B 2019 *Chin. Phys. B* **28** 77501

[46] Ma Y R, Li L J and Duan W S 2019 *Chin. Phys. B* **28** 25201

[47] Bains A S, Misra A P, Saini N S and Gill T S 2010 *Phys. Plasmas* **17** 012103

[48] Marklund M, Eliasson B and Shukla P K 2006 *Phys. Plasmas* **13** 083102

[49] Shukla P K, Stenflo L and Fedele R 2003 *Phys. Plasmas* **10** 310

[50] Shatashvili N L, Javakhishvili J I and Kaya H 1997 *Astrophys. Space Sci.* **250** 109

[51] Zakharov V E and Ostrovsky L A 2009 *Physica D* **238** 540

[52] Meier J, Stegeman G I, Christodoulides D N, Silberberg Y, Morandotti R, Yang H, Salamo G, Sorel M and Aitchison J S 2004 *Phys. Rev. Lett.* **92** 163902

[53] Reece P J, Wright E M and Dholakia K 2007 *Phys. Rev. Lett.* **98** 203902

[54] Lontano M, Bulanov S V, Koga J, Passoni M and Tajima T 2002 *Phys. Plasmas* **9** 2562

[55] Eliasson B and Shukla P K 2006 *Phys. Lett. A* **354** 453

[56] Borhanian J 2012 *Phys. Plasmas* **19** 082306

[57] Cattaert T, Kourakis I and Shukla P K 2005 *Phys. Plasmas* **12** 012319

[58] Borhanian J, Kourakis I and Sobhanian S 2009 *Phys. Lett. A* **373** 3667

[59] Lee N C 2011 *Phys. Plasmas* **18** 062310

[60] Hadžievski Lj, Jovanović M S, Škorić M M and Mima K 2002 *Phys. Plasmas* **9** 2569

[61] Lehmann G, Laedke E W and Spatschek K H 2006 *Phys. Plasmas* **13** 092302

[62] Saxena V, Das A, Sengupta S, Kaw P and Sen A 2007 *Phys. Plasmas* **14** 072307

[63] Saxena V, Das A, Sen A and Kaw P 2006 *Phys. Plasmas* **13** 032309

[64] Saxena V, Kourakis I, Sánchez-Arriaga G and Siminos E 2013 *Phys. Lett. A* **377** 473

[65] Rostampooran S and Aslaninejad M 2017 *Phys. Plasmas* **24** 042302

[66] Holkundkar A R and Brodin G 2018 *Phys. Rev. E* **97** 043204

[67] Sharma A, Malik H K, Kumar H and Goyal S 2019 *J. Appl. Phys.* **13** 31

[68] Sharma A, Malik H K and Kumar H 2018 *J. Appl. Phys.* **12** 65

[69] Hong X R, Zhou W J, Xie B S, Yang Y, Wang L, Tian J M, Tang R A and Duan W S 2017 *Chin. Phys. B* **26** 065203

[70] Wang H Y, Sun P, Jiang W, Zhou J and Xie B S 2014 *Chin. Phys. B* **24** 065207

[71] Weng S M, Murakami M, Mulser P and Sheng Z M 2012 *New J. Phys.* **14** 063026

[72] Dawson J M 1983 *Rev. Mod. Phys* **55** 403

[73] Pan K Q, Li S W, Guo L, Yang D, Li Z C, Zheng C Y, Jiang S E, Zhang B H and He X T 2018 *Phys. Plasmas* **25** 052301

[74] Wu D, Yu W, Fritzsche S, Zheng C Y and He X T 2019 *Phys. Plasmas* **26** 063107

[75] Hashemzadeh M and Niknam A R 2017 *Phys. Plasmas* **24** 062102

[76] Chen H Y, Liu S Q and Li X Q 2011 *Opt. Int. J. Light Electron. Opt.* **122** 599
[77] Borhanian J and Aghaei G H 2017 *Phys. Plasmas* **24** 033116
[78] Zheng X L, Weng S M, Zhang Z, Ma H H, Chen M, Mckenna P and Sheng Z M 2019 *Opt. Express* **28** 15794
[79] Zhao Y, Weng S M, Sheng Z M, Kang N, Liu H Y, Zhu J Q and Zhang J 2020 *Opt. Express* **27** 19319
[80] Farina D, Lontano M and Bulanov S 2000 *Phys. Rev. E* **62** 4146
[81] Tang R A, Hong X R, Gao J M and Xue J K 2016 *Phys. Lett. A* **380** 1037
[82] Tang R A, Cheng R J, Hong X R, Liu T F, Li X X, Gao J M, Guo P, Tian J M and Xue J K 2020 *Phys. Lett. A* **384** 126267
[83] Fedele R and Schamel H 2002 *Eur. Phys. J. B* **27** 313
[84] Shukla P K, Bharuthram R and Tsintsadze N L 1987 *Phys. Rev. A* **35** 4889